Article

Synthesis, Characterization, and Application of Europium(III) Complexes as Luminescent Markers of Banknotes

Clebson J. Macrino,[a,b] Elias M. Silva,[a] Victor R. Cunha,[c] Victor R. Fonseca,[a] Álvaro Cunha Neto,[a]
Joyce R. Araújo,[c] Valdemar Lacerda Jr. *,[a] and Wanderson Romão *,[a,b,d]

[a]*Laboratório de Petroleômica e Forense, Universidade Federal do Espírito Santo (UFES),
Avenida Fernando Ferrari, 514, Goiabeiras, 29075-910 Vitória-ES, Brazil*

[b]*Instituto Nacional de Ciências e Tecnologia Forense (INCT Forense),
Av. Ipiranga, 6681, Partenon, 90619-900 Porto Alegre-RS, Brazil*

[c]*Divisão de Metrologia de Materiais, Instituto Nacional de Metrologia, Qualidade e Tecnologia,
Av. Nossa Senhora das Graças, 50, 25250-020 Duque de Caxias-RJ, Brazil*

[d]*Instituto Federal do Espírito Santo (IFES), Av. Ministro Salgado Filho, Soteco,
29106-010 Vila Velha-ES, Brazil*

In this work, three complexes were synthesized from the trivalent europium ion (Eu[III]), using the picrate anion (pic), and delta-valerolactam (DVL), epsilon-caprolactam (EPK), and oenantholactam (OEN). The synthesized complexes [Eu(pic)$_3$·(DVL)$_3$], [Eu(pic)$_3$·(EPK)$_3$], and [Eu(pic)$_3$·(OEN)$_3$] were studied as luminescent markers for application as security elements in Brazilian banknotes. All complexes showed red color emission with absorption at 397 nm and emission at 614 nm. Qualitative luminescence tests were performed on R$10, R$20, R$50, and R$100 Brazilian banknotes. The complexes were applied on the surface of the banknotes and were exposed to different wavelengths of 254, 312, 365, and 320-400 nm. The chemical profiles of the complexes were identified on the banknotes employing the laser desorption ionization mass spectrometry (LDI (±) MS) technique. Generally, tests were promising, and can thus provide a simple, fast, and easy method to identify the authenticity of questioned documents, with an average cost of R$0.65 *per* mg.

Keywords: counterfeiting, luminescent markers, europium(III) complexes, LDI MS

Introduction

Documentoscopy or detection of forgery is the branch of forensic chemistry dealing with the study of questioned documents to verify their authenticity. It has a role in criminalistics, not only to determine the veracity of documents but also to discover the authorship of falsifications and the means that were employed.[1-3]

The falsification of documents is characterized as a crime of intelligence, and within the field of documentoscopy, banknotes, stamps, national driving licenses, identity cards, vehicle registration certificates, vehicle licensing certificates, credit cards, and checks stand out as primary targets of frauds.[4] Within this context, the use of different analytical techniques is reported in the literature to determinate authenticity, such as gas chromatography

coupled to mass spectrometry (GC-MS) and Fourier transform infrared (FTIR) spectroscopy to determine the ages of documents,[5,6] video spectral comparator (VSC) to establish trace release order,[7] and ultraviolet-visible (UV-Vis) spectroscopy for the differentiation of italic letters.[8]

The advancement of digital technologies in copying equipment, printing, and image processing has facilitated the falsification of documents, and the quality of falsified documents can be practically indistinguishable from the original document.[9] Therefore, the development of efficient and rapid analytical techniques to determine authenticity is necessary. Typically, the techniques used include atomic force microscopy,[10] FTIR spectroscopy,[11] Raman spectroscopy,[12-14] GC-MS,[15] ESI MS (electrospray ionization mass spectrometry),[16] LDI MS (laser desorption ionization mass spectrometry),[17-19] and ambient ionization mass spectrometry techniques EASI MS (easy ambient

*e-mail: vljuniorqui@gmail.com; wandersonromao@gmail.com

sonic-spray ionization mass spectrometry), PSI MS (paper spray ionization mass spectrometry), DESI MS (desorption electrospray ionization mass spectrometry), and DART MS (direct analysis in real time mass spectrometry).[20-24] Among the types of forgery employed, the counterfeiting of banknotes deserves particular attention, since this is an increasingly common financial crime, both in the sense of increasing the number of falsified records and in the diversity of the falsification methods used by the falsifiers.[25,26] In addition, this type of crime can affect the economy of several countries. Therefore, the use of efficient security items such as security papers, latent images, watermarks, magnetic strips, special printing techniques, holograms, and areas with infrared (IR) or ultraviolet (UV) light responses has been adopted as a form of fingerprinting for authentic banknotes.[27]

It is of great importance to use security items that are easily and quickly identified by the population to prevent counterfeiting of banknotes. For this purpose, the use of new photoluminescent materials that emit light in the presence of electromagnetic radiation in the IR or UV region gains prominence because these materials meet the requirement of simple and rapid identification. New materials incorporating lanthanides[28-37] may be potential photoluminescent markers for the authenticity of banknotes.

The luminescent property of lanthanide ions mainly originates from transitions involving partially occupied 4f orbitals. The luminescence phenomenon using direct excitation of the lanthanide ion is inefficient because it does not have high molar absorptivity. The light is absorbed by an organic molecule (ligand), which transfers energy to the lanthanide ion, which then emits luminescence resulting from intra-configuration transitions of orbital 4f and usually observed in the visible region. Hence, there is an intra-molecular energy transfer from the ligand to the metal ion known as the "antenna effect".[38,39]

This luminescent ability of the lanthanide complexes, to absorb and emit radiation with characteristic wavelengths, defines these materials as light conversion molecular devices (DMCLs). The efficiency of the transfer of energy from the binder to the lanthanide ion depends on the chemical nature of the coordinated ligand.[40] Among the lanthanide(III) ions, the elements europium, terbium, and thulium emit in the regions of visible red, green, and blue light, respectively.[41,42] The luminescent properties of materials derived from these metals have broad applicability in several areas, including their use as bio-detectors,[43,44] films,[45] solar cells,[46] and organic light-emitting diode (OLED),[47] and, in the forensic field, in the detection of explosives,[28] fingerprints,[48,49] and gunshot residues.[50,51]

A series of lanthanide(III) picrate (pic) complexes with different organic molecules as coligands are reported in the literature. Silva *et al.*[52] described the preparation of a complex isomorphous with hexamethylphosphoramide (HMPA), with the formula $[Ln(pic)_3 \cdot (HMPA)_3]$ (Ln = Nd, Eu). Miranda Jr. *et al.*[53] reported the characterization of the structure with composition $[Ln(pic)_3 \cdot (DTSO)_3]$ (Ln = La-Yb, Y), using 1,3-dithiane-1-oxide (DTSO) as a coligand. Melo *et al.*[54] synthesized lanthanide(III) picrate complexes with *N,N*-dimethylacetamide (DMA), with the composition $[Ln(pic)_3 \cdot (DMA)_3]$ (Ln = La, Eu, Gd, Sm, Lu). Nunes *et al.*[55] reported a complex with 3-picoline-*N*-oxide (3-picNO) and the formula $[Eu(pic)_3 \cdot (3\text{-}picNO)_2 \cdot (H_2O)]$. Marinho *et al.*[56] described a synthesis utilizing pyrazine-*N*-oxide (pyzNO) obtaining compounds with the composition $[Ln(pic)_3 \cdot (pyzNO)_2 \cdot (H_2O)_7]$ (Ln = Nd, Eu). Destefani *et al.*[57] reported a compound using *N*-methylcaprolactam (NMK) as coligand with the formula $[Eu(pic)_3 \cdot (NMK)_3]$.

This work reports the synthesis, characterization, and application of three new europium(III) picrate complexes, using three different lactams (delta-valerolactam, epsilon-caprolactam, and oenantholactam) as coligands, for luminescent markers of Brazilian R$10, R$20, R$50, and R$100 banknotes.

Experimental

Materials

Ethanol, hydrochloric acid (HCl), ethylenediamine-tetraacetic acid (EDTA) and urea (analytical grade with purity higher than 99.5%) were supplied by Vetec Química Fina Ltda, Duque de Caxias, RJ, Brazil. Eu_2O_3 (99.9%), picric acid (pic) $C_6H_3N_3O_7$ (99.9%), delta-valerolactam (DVL) C_5H_9NO (98%), epsilon-caprolactam (EPK) $C_6H_{11}NO$ (98%), and oenantholactam (OEN) $C_7H_{13}NO$ (98%) were supplied by Sigma-Aldrich Chemicals, St. Louis, USA.

The chemical stoichiometry of the complexes was determined through complexometric titration with 0.01 mol L^{-1} EDTA standard solution[58] and elemental analysis using a Thermo Fisher Scientific Flash 1112-CHNS-O (Waltham, Massachusetts, USA). The infrared spectra were obtained in transmittance mode with an attenuated total reflectance accessory (ATR) in the region of 4000-650 cm^{-1}, using a PerkinElmer FTIR Spectrum 400 MID/NIR spectrometer (Waltham, Massachusetts, USA) at room temperature. UV-Vis region spectroscopy analyses were performed for the solid-state complexes using a PerkinElmer spectrometer (Waltham, Massachusetts, USA), in the range of 220-800 nm. Excitation spectra were obtained at room temperature in the

range of 250-550 nm, with a slot opening of 0.75, monitoring the intensity of the $^5D_0 \rightarrow {}^7F_2$ transition at 616 nm. Emission spectra were obtained in the range of 550-750 nm at room temperature, with a slot opening of 0.75 and excitation at 397 nm, using a Quanta Master 40 spectrofluorometer (Edison, New Jersey, USA) with a 75 W xenon lamp. Determinations of the exact masses of the complexes were made by laser desorption ionization mass spectrometry in both ionization modes, LDI ($\pm$) MS, using an FT-ICR model 9.4 T Solarix mass spectrometer, Bruker Daltonics (Bremen, Germany), equipped with a Smartbeam-II™ (355 nm) laser. LDI ($\pm$) MS data were acquired with 16 scans with a frequency of 200 Hz in the range of *m/z* 200-1200, using 100 laser shots *per* pixel, a small (ca. 30 μm) laser focus setting, and laser power ranging from 13 to 15%.

Synthesis

Synthesis of hydrated europium(III) picrate [Eu(pic)$_3$·(H$_2$O)$_{11}$]

Initially, hydrated basic carbonate of europium(III), EuCO$_3$(OH)·xH$_2$O, was obtained from Eu$_2$O$_3$ (5.0 g) and concentrated hydrochloric acid was added to the oxide suspension in water (800 mL). The solution was heated (85-90 °C) and urea was added until the solution reached a pH of approximately 7. Basic carbonate hydrate of europium(III) with a yield of 91% was obtained as a product, and 2.0 g of this compound was then suspended in an aqueous medium (100 mL). This solution was heated (85-90 °C) and picric acid was added until all basic carbonate was consumed. The resulting solution was filtered and allowed to stand at room temperature for crystallization. The obtained crystals had yellow coloration and were dried at room temperature and stored in an amber bottle.[59] Yield 79%; anal. calcd. (%) for [Eu(pic)$_3$·(H$_2$O)$_{11}$]: C 20.90, H 2.73, N 12.19, Eu^{III} 14.70, found: C 20.60, H 2.50, N 11.83, Eu^{III} 15.50; FTIR-ATR ν / cm^{-1} 1558$_{(s)}$

$ν_{ass}$NO$_2$, 1335$_{(s)}$ $ν_s$NO$_2$, 797$_{(m)}$ $γ$CH, for free picric acid (Figure 1a) 1526$_{(s)}$ $ν_{ass}$NO$_2$, 1539$_{(s)}$ $ν_s$NO$_2$, 782$_{(m)}$ $γ$CH.

Synthesis of complexes

The compounds were prepared by dissolving the hydrated europium(III) picrate in ethanol with an ethanolic solution of the lactam (molar ratio 1:3, lactam = DVL, EPK, and OEN). Triethyl orthoformate, which is used as a dehydrating agent, was then added, contributing to the removal of hydration waters from the europium(III) picrate. The system was stirred until a yellow solid appeared. The solid obtained was washed with ethyl ether, dried at room temperature, and stored in an amber bottle.[60] The results of experimental and calculated elemental analysis and FTIR analysis of the complexes were as follows:

Europium(III) picrate with delta-valerolactam [Eu(pic)$_3$·(DVL)$_3$]

Yield 63%; anal. calcd. (%) for C$_{33}$H$_{33}$N$_{12}$O$_{24}$Eu: C 34.87, H 2.93, N 14.79, Eu^{III} 13.40, found: C 35.88, H 3.09, N 14.39, Eu^{III} 13.37; FTIR-ATR ν / cm^{-1} (Figure 1c) 2956$_{(s)}$ $ν$NH, 1599$_{(s)}$ $ν$C=O, 1534$_{(s)}$ $ν_{ass}$NO$_2$, 1318$_{(s)}$ $ν_s$NO$_2$, 785$_{(m)}$ $γ$CH, for free DVL (Figure 1b) 2951$_{(s)}$ $ν$NH, 1637$_{(s)}$ $ν$C=O.

Europium(III) picrate with epsilon-caprolactam [Eu(pic)$_3$·(EPK)$_3$]

Yield 68%; anal. calcd. (%) for C$_{36}$H$_{39}$N$_{12}$O$_{24}$Eu: C 36.69, H 3.33, N 14.26, Eu^{III} 12.93, found: C 37.39, H 3.39, N 14.34, Eu^{III} 13.01; FTIR-ATR ν / cm^{-1} (Figure 1e) 2935$_{(s)}$ $ν$NH, 1607$_{(s)}$ $ν$C=O, 1534$_{(s)}$ $ν_{ass}$NO$_2$, 1324$_{(s)}$ $ν_s$NO$_2$, 790$_{(m)}$ $γ$CH, for free EPK (Figure 1d) 2930$_{(s)}$ $ν$NH, 1647$_{(s)}$ $ν$C=O.

Europium(III) picrate with oenantholactam [Eu(pic)$_3$·(OEN)$_3$]

Yield 72%; anal. calcd. (%) for C$_{39}$H$_{45}$N$_{12}$O$_{24}$Eu: C 38.43, H 3.69, N 13.79, Eu^{III} 12.48, found: C 38.46,
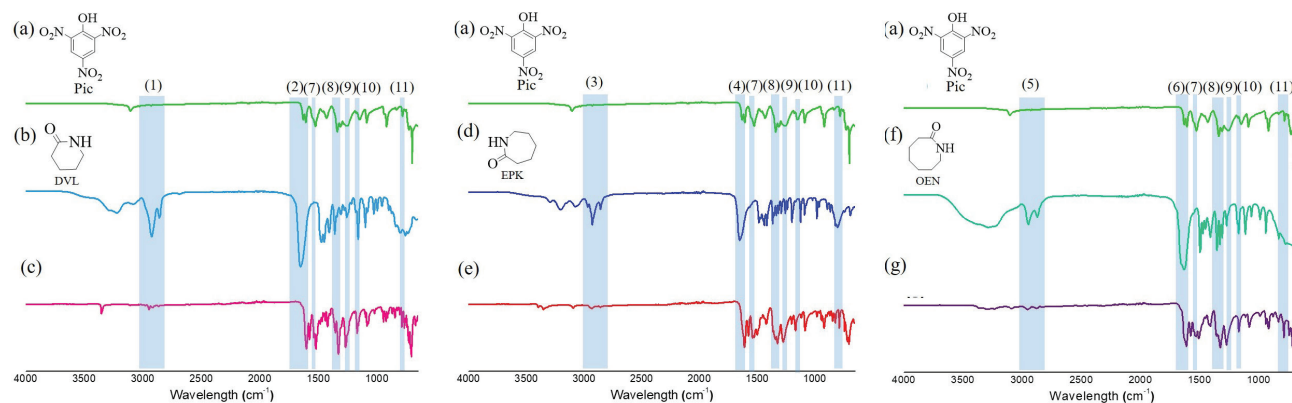
Figure 1. FTIR-ATR spectra of (a) pic: $ν_{ass}$NO$_2$ (7), $ν_{as}$NO$_2$ (8), $ν$C–O (9), $γ$OH (10), $γ$CH (11); (b) DVL: $ν$NH (1), $ν$C=O (2); (c) [Eu(pic)$_3$·(DVL)$_3$]: $ν$NH (1), $ν$C=O (2), $ν_{ass}$NO$_2$ (7), $ν_{as}$NO$_2$ (8), $ν$C–O (9), $γ$CH (11); (d) EPK: $ν$NH (3), $ν$C=O (4); (e) [Eu(pic)$_3$·(EPK)$_3$]: $ν$NH (3), $ν$C=O (4), $ν_{ass}$NO$_2$ (7), $ν_{as}$NO$_2$ (8), $ν$C–O (9), $γ$CH (11); (f) OEN: $ν$NH (5), $ν$C=O (6); (g) [Eu(pic)$_3$·(OEN)$_3$]: $ν$NH (5), $ν$C=O (6), $ν_{ass}$NO$_2$ (7), $ν_{as}$NO$_2$ (8), $ν$C–O (9), $γ$CH (11).

H 3.70, N 13.80, Eu^{III} 12.40; FTIR-ATR ν / cm^{-1} (Figure 1g) 2940$_{(s)}$ νNH, 1604$_{(s)}$ νC=O, 1554$_{(s)}$ ν$_{ass}$NO$_2$, 1335$_{(s)}$ ν$_s$NO$_2$, 783$_{(m)}$ γCH, for free OEN (Figure 1f) 2924$_{(s)}$ νNH, 1655$_{(s)}$ νC=O.

The syntheses of the three complexes are represented schematically in Figure 2.

Application of complexes in Brazilian banknotes

A total of six Brazilian banknotes were used: one each in the values of R$10, R$20, and R$100, and three R$50 notes. The notes were purchased from a Brazilian bank. The R$10 and R$20 banknotes were chosen because they are more commonly used; the R$50 and R$100 banknotes were chosen because they have greater value and are major targets of counterfeiting. For the R$50 banknotes, approximately 1 mg of each complex was applied using a swab and deposited on the surface of the banknotes at the top of the region that contained the value of each banknote. Later, the complex that showed the best photoluminescence (in this case the [Eu(pic)$_3$·(EPK)$_3$]) was applied to the other three (i.e., R$10, R$20, and R$100) banknotes. Complexes were applied to the areas showing the respective monetary values of the banknotes. Qualitative analyses of the photoluminescence were evaluated using a Video Spectral Comparator VSC® 6000 (Foster & Freeman, Worcestershire, United Kingdom), operated at 254, 312 and 365 nm, and a Lumatec Superlite 400 (Deisenhofen, Germany), with excitation between 320-400 nm.

Results and Discussion

Synthesis

Hydrated basic carbonates of europium(III) were prepared by precipitation from homogeneous solutions via the hydrolysis of urea without the addition of an auxiliary anion,[61] allowing the formation of hydrated europium(III) picrate by the direct reaction of hydrated basic carbonate of europium(III) with picric acid. This process obtained a high yield and a non-hygroscopic compound.

The stoichiometry of the complexes was obtained through elemental analysis (CHN), which confirmed the 1:3 molar ratio ([Eu(pic)$_3$·(H$_2$O)$_{11}$]:lactam). FTIR spectra (Figure 1) identified the presence of asymmetric stretching frequencies (ν$_{ass}$NO$_2$ (region 7)) and symmetrical frequencies (ν$_s$NO$_2$ (region 8)) for the picrate ion, demonstrating the coordination of this ion to the metallic center of the europium(III). The split and shifted ν$_s$NO$_2$ vibration suggested that the picrate ions are coordinated to the metallic center in a bidentate form, through the phenolic oxygen atom and the *o*-nitro group oxygen atom. The disappearance of the out-of-plane vibration of the OH (region 10) group at 1151 cm^{-1}, corresponding to free picric acid, indicates that hydrogen has been replaced by the Eu^{III} ion and that phenolic oxygen coordination to Eu^{III} has occurred. The νC–O (region 9) vibration shift from 1260 to 1274 cm^{-1} suggests that the substitution of phenolic hydrogen (OH) by Eu^{III} increases the π character of the C–O bond.[62-64] In addition, the νC=O (regions 2, 4, and
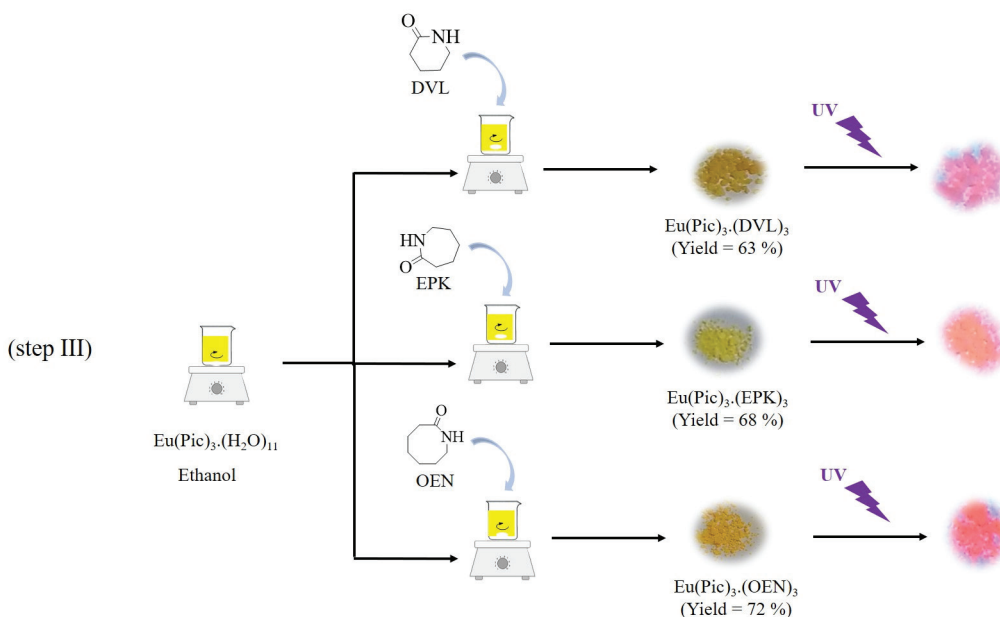

Figure 2. Scheme of the syntheses of the studied Eu^{III} complexes.

6) vibration shift for lower energy regions and decreased intensity of νNH (regions 1, 3, and 5) stretching of lactams, concerning the free ligand, suggests the coordination of carbonyl to the Eu^{III} ion.[65]

Emission and excitation analysis

The UV-Vis absorption spectra of [Eu(pic)$_3$·(DVL)$_3$] in Figure S1a (Supplementary Information (SI) section) and [Eu(pic)$_3$·(EPK)$_3$] complexes in Figure S1c (SI section) show bands with maximum absorption at 323 and 324 nm, respectively, which can be attributed to intra-ligand $\pi \rightarrow \pi^*$-type electronic transitions, and a band with maximum intensity at 391 nm, which was observed for both, attributed to $n \rightarrow \pi^*$-type transitions. For the [Eu(pic)$_3$·(OEN)$_3$] complex in Figure S1b (SI section), a single broad band with a maximum intensity at 361 nm was observed and can be attributed to the overlapping $\pi \rightarrow \pi^*$ and $n \rightarrow \pi^*$ transitions. In addition, a low-intensity band around 740 nm was observed for all complexes and is assigned to the f-f transitions of the $^7F_5 \rightarrow {}^5D_0$ type for the Eu^{III} ion.[66]

The excitation spectra in Figure S2 (SI section) presented a broad band between 250-500 nm, which can be attributed to the central ligand (maximum at 397 nm) and characterized as the transition band of the ligands ($S_0 \rightarrow S_1$). The excitation at 397 nm is very close to the $^5L_6$ level of the Eu^{III} (394 nm). The excitation spectra exhibit a broad band between 250-500 nm, overlapping the $^5L_6$ level. Therefore, the $^5L_6$ level can also be an efficient channel for the photoluminescence of the compounds, although lanthanide ions have low absorption coefficients.

The emission spectra in Figure 3 of the compounds at room temperature showed the regions of the f-f transitions from the excited level $^5D_0 \rightarrow {}^7F_J$ (J = 0, 1, 2, 3, and 4): $^5D_0 \rightarrow {}^7F_0$ (576 nm), $^5D_0 \rightarrow {}^7F_1$ (590 nm), $^5D_0 \rightarrow {}^7F_2$ (614 nm), $^5D_0 \rightarrow {}^7F_3$ (650 nm), and $^5D_0 \rightarrow {}^7F_4$ (696 nm), with maximum emission at 614 nm. The band corresponding to the $^5D_0 \rightarrow {}^7F_0$ transition was observed to have weak intensity. The presence of this band suggests that the Eu^{3+} ion is involved in a low-symmetry chemical environment, which may be of C_n, C_s, or C_{nv} type.[67] The $^5D_0 \rightarrow {}^7F_2$ transition is a hypersensitive transition with a predominantly electric dipole character, and when its intensity is higher than that of the $^5D_0 \rightarrow {}^7F_1$ transition, this indicates that the compounds have no inversion center. The low intensity of the $^5D_0 \rightarrow {}^7F_0$ transition associated with the intensity presented by the $^5D_0 \rightarrow {}^7F_4$ transition can be interpreted in terms of the symmetry of the Eu^{III} ion chemical environment, suggesting that it is in a highly polarizable chemical environment with distorted symmetry.[68] The experimental intensity parameters Ω_λ

($\lambda = 2$ and 4) in Table 1 were determined from the emission spectra for the compounds based on the $^5D_0 \rightarrow {}^7F_2$ and $^5D_0 \rightarrow {}^7F_4$ transitions, with the $^5D_0 \rightarrow {}^7F_1$ magnetic-dipole-allowed transition as the reference because this transition is practically insensitive to changes in the chemical environment. They are estimated according to equation 1:[69]

$$\Omega_\lambda = \frac{3\hbar c^3 A_{0 \rightarrow J}}{4e^2\omega^3\chi\left\langle {}^5D_0 \left\| U^{(\lambda)} \right\|^7 F_J \right\rangle^2} \tag{1}$$

where e is the electronic charge, ω is the angular frequency of the transition, $\hbar$ is Planck's constant divided by 2π, c is the velocity of light, and $\chi = n(n^2 + 2)^2/9$ is the Lorentz local field correction term with a refraction index n of 1.5. The squared reduced matrix elements are $\langle {}^5D_0\|U^{(2)}\|{}^7F_2\rangle^2 = 0.0032$ and $\langle {}^5D_0\|U^{(4)}\|{}^7F_4\rangle^2 = 0.0023$.[70,71] The Ω_6 parameter was not determined because the $^5D_0 \rightarrow {}^7F_6$ transition could not be experimentally detected. It occurs in the near IR (ca. 840 nm) and thus beyond the detection range of the experimental setup. The Ω_2 and Ω_4 intensity parameters for the complexes are presented in Table 1. In this case, the Einstein coefficient values of spontaneous emission between $^5D_0 \rightarrow {}^7F_J$ ($A_{0\lambda}$) are obtained using equation 2:

$$A_{0\lambda} = A_{01} \frac{S_{0\lambda}}{S_{01}} \frac{\nu_{01}}{\nu_{0\lambda}} \tag{2}$$

where $S_{0\lambda}$ is the area under the emission curve related to the $^5D_0 \rightarrow {}^7F_J$ transitions obtained from the spectral data, and $\nu_{0\lambda}$ is the energy barycenter of the transitions from the $^5D_0$ excited state to the $^7F_1$, $^7F_2$, and $^7F_4$ ground states (in cm^{-1}). The $^5D_0 \rightarrow {}^7F_1$ magnetic-dipole-allowed transition is almost independent of the crystal field environment around the Eu^{III} ion (the A_{01} value is estimated to be approximately 50 s^{-1}).[72]

Table 1. Experimental intensity parameters Ω_2 and Ω_4 calculated for the compounds

Compound	Ω_2 / (10^{-20} cm^2)	Ω_4 / (10^{-20} cm^2)
[Eu(pic)$_3$·(H$_2$O)$_{11}$]	11.38	7.45
[Eu(pic)$_3$·(DVL)$_3$]	16.17	7.41
[Eu(pic)$_3$·(EPK)$_3$]	17.90	7.15
[Eu(pic)$_3$·(OEN)$_3$]	15.76	7.29

pic: picrate anion; DVL: delta-valerolactam; EPK: epsilon-caprolactam; OEN: oenantholactam.

The experimental intensity parameter Ω_2 shows different values for the compounds in Table 1, indicating that the Eu^{III} ions are in different chemical environments and that
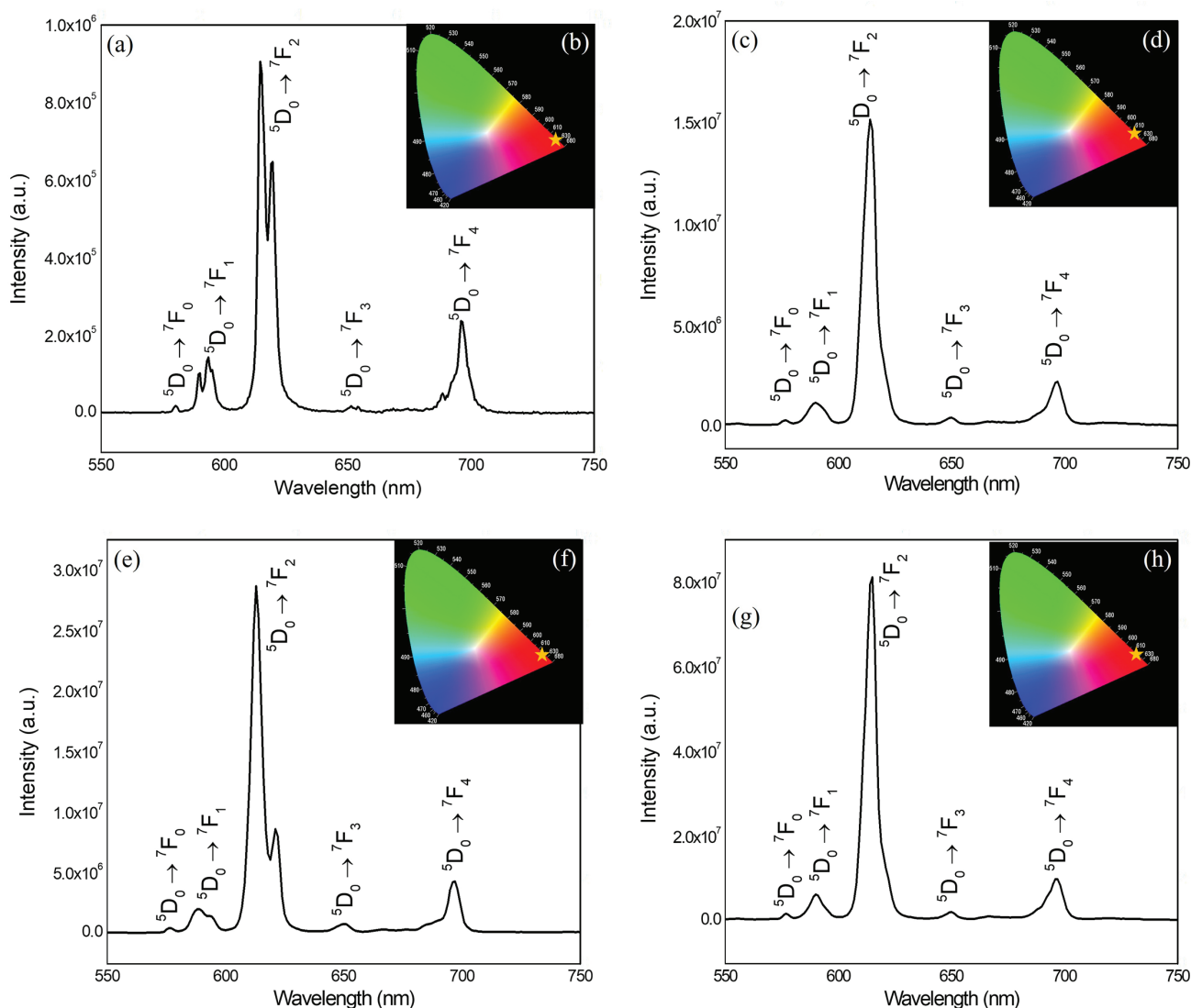
Figure 3. Emission spectra at room temperature, $\lambda_{exc.}$ = 397 nm, of (a) [Eu(pic)$_3$·(H$_2$O)$_{11}$], (c) [Eu(pic)$_3$·(DVL)$_3$], (e) [Eu(pic)$_3$·(EPK)$_3$], and (g) [Eu(pic)$_3$·(OEN)$_3$] and their respective chromaticity diagrams: (b) [Eu(pic)$_3$·(H$_2$O)$_{11}$], (d) [Eu(pic)$_3$·(DVL)$_3$], (f) [Eu(pic)$_3$·(EPK)$_3$], and (h) [Eu(pic)$_3$·(OEN)$_3$].

a highly polarizable chemical environment exists around the Eu^{III}. According to the literature,[73] the Ω_2 value is most influenced by small angular changes in the local geometry. This effect, together with changes in the polarizability of the ligating atom (α), has been used to explain the hypersensitivity of certain 4f-4f transitions to changes in the chemical environment. Borges *et al.*[74] reported a new anionic complex containing 1-ethyl-3-methylimidazolium (EMIm) with the composition (EMIm)$_2$[Eu(Pic)$_4$·(H$_2$O)$_2$]Pic and found values for Ω_2 (16.7 × 10^{-20} cm^2) and Ω_4 (7.7 × 10^{-20} cm^2). This is consistent with the values found for Ω_2 and Ω_4 in the present study for the compounds.

The red color of the synthesized compounds was verified using the chromaticity diagram in Figure 3 generated by the Spectra Lux 1.0 software,[75] which used the emission spectra between 550-750 nm. The following coordinates

were obtained: (x = 0.68; y = 0.31) for [Eu(pic)$_3$·(H$_2$O)$_{11}$] in Figure 3b, (x = 0.67; y = 0.32) for [Eu(pic)$_3$·(DVL)$_3$] in Figure 3d, (x = 0.68; y = 0.32) for [Eu(pic)$_3$·(EPK)$_3$] in Figure 3f, and (x = 0.68; y = 0.32) for [Eu(pic)$_3$·(OEN)$_3$] in Figure 3h. The values found for the chromaticity coordinates are in agreement with the standard values for red luminophores (x = 0.64; y = 0.33).[75,76]

Photoluminescence analyses were qualitatively performed on the banknotes to visually assess the light emission of each complex present on the R$50 banknotes. Figure 4 shows the light emission of each complex under excitation at different wavelengths.

The emission of red light, corresponding to each complex present in the banknotes, under excitation at different wavelengths (254, 312, 365, and 320-400 nm (Lumatec Spritelite 400)) was easily visualized. These excitation
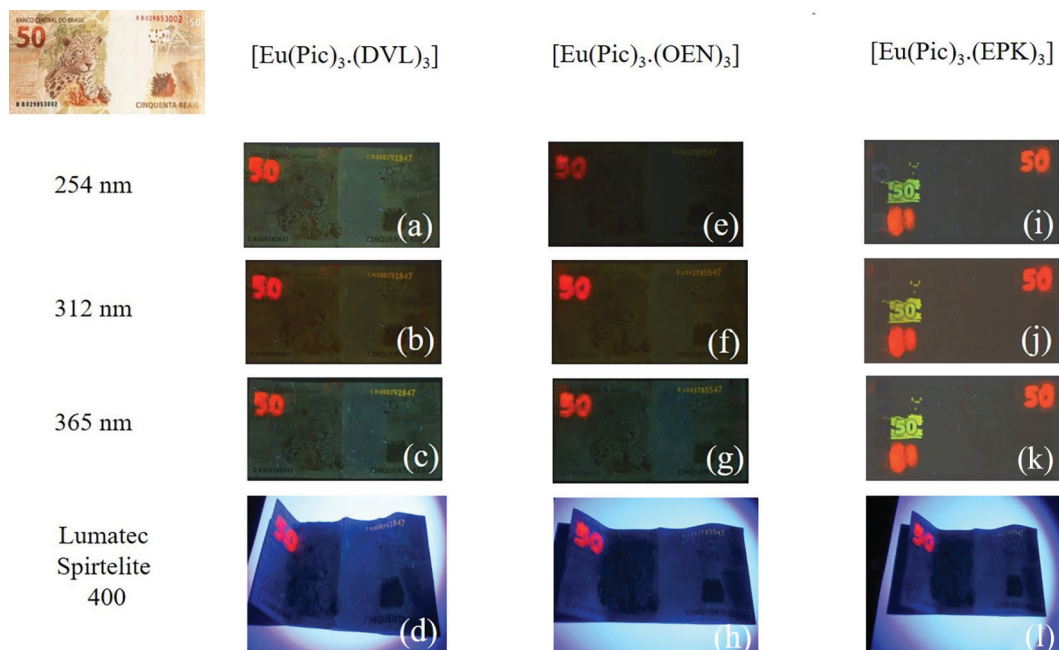
Figure 4. R$50 banknotes marked with three studied complexes under excitation at different wavelengths (254, 312, 365, and 320-400 nm).

wavelengths were visually evaluated by observation of the emitted light from the complexes. At 365 and 320-400 nm, which are wavelengths close to that obtained in the excitation spectra (397 nm), the observed red light emission was more intense than that at the 254 and 312 nm wavelengths. In addition to the luminescence from the complexes added to the banknote surfaces, Figures 4i-4k also show a region of emitted green light, which is attributable to one of the security elements already present in the banknote itself.

While all the complexes produced light emissions that allowed their visual identification on banknotes, the [Eu(pic)$_3$·(EPK)$_3$] complex was selected and applied on the surface of the R$10, R$20, and R$100 banknotes. Figure 5 shows the red light emission of the [Eu(pic)$_3$·(EPK)$_3$] complex under excitation at different wavelengths on the R$10, R$20, and R$100 banknotes.

Based on the results in Figure 5, it was observed that the luminescence of the [Eu(pic)$_3$·(EPK)$_3$] is visually

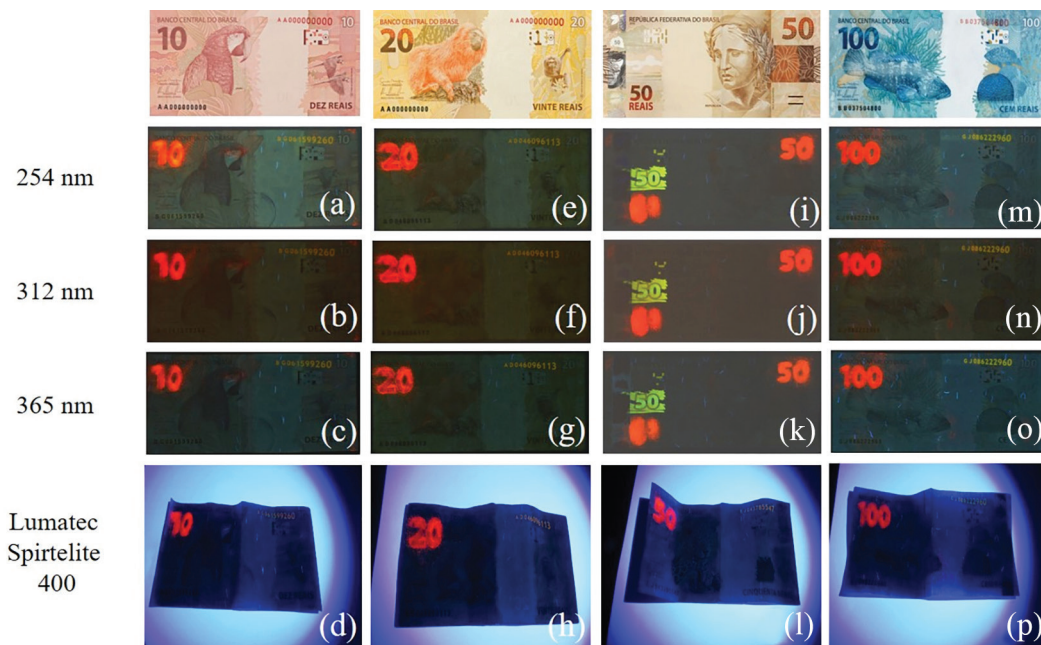**Figure 5.** R$10, R$20, R$50 and R$100 banknotes marked with 1 mg [Eu(pic)$_3$·(EPK)$_3$] under excitation at different wavelengths (λ = 254, 312, 365, and 320-400 nm).

noticeable at different wavelengths. The 365 nm wavelength emits more intense luminescence because it is closer to the maximum excitation wavelength (397 nm) of the [Eu(pic)$_3$·(EPK)$_3$] complex.

LDI (±) MS

To identify the chemical profile of the complexes deposited on the banknote surfaces while preserving their integrity, the LDI (±) MS technique was used, in which an analysis is made from the incidence of a laser beam (which may be pulsed ultraviolet or IR) focusing on a surface, allowing analyte desorption and ionization without the necessity of previous sample preparation.[77-80] Figures 6a-6d show the chemical profile of R\$50 banknotes obtained by LDI (+) MS (Figure 6a) without Eu^{III} complexes, and with (Figure 6b) [Eu(pic)$_3$·(DVL)$_3$], (Figure 6c) [Eu(pic)$_3$·(EPK)$_3$], and (Figure 6d) [Eu(pic)$_3$·(OEN)$_3$].

Figure 6a shows the chemical profile of the banknote with no complexes applied. It was observed that an ion of

m/z 575.08132 is present. This ion is found abundantly in different regions of the R\$50 banknotes before application of the complexes and thus can be characterized as a natural chemical marker to recognize the authenticity of banknotes. Eberlin *et al.*[22] reported an analysis of Brazilian banknotes using DESI MS and EASI MS, identifying ions of *m/z* 391, 413, 429, 803 and 819 as natural markers that characterize the chemical profile of the authentic banknotes. Schmidt *et al.*[81] also reported the study of a second family of real banknotes using EASI (+) MS, where the ion of *m/z* 443 was used as a fingerprint of authenticity.

LDI (+) MS spectra in Figures 6a-6d were obtained with mass resolution m/Δm$_{50\%}$ ca. 381783, where Δm$_{50\%}$ is the full peak width at half-maximum peak height and *m/z* ca. 400,[82] and showed mass errors ranging from 0.76 to 4.64 ppm as shown in Table 2. For the [Eu(pic)$_3$·(DVL)$_3$] complex, with molecular formula (M) = EuC$_{33}$H$_{33}$N$_{12}$O$_{24}$ and molecular weight (M$_w$) = 1134 Da, LDI (+) MS analysis (Figure 6b) showed a signal representing the ion of *m/z* 906.10605, [EuC$_{27}$H$_{31}$N$_9$O$_{17}$]$^+$, double bond equivalent
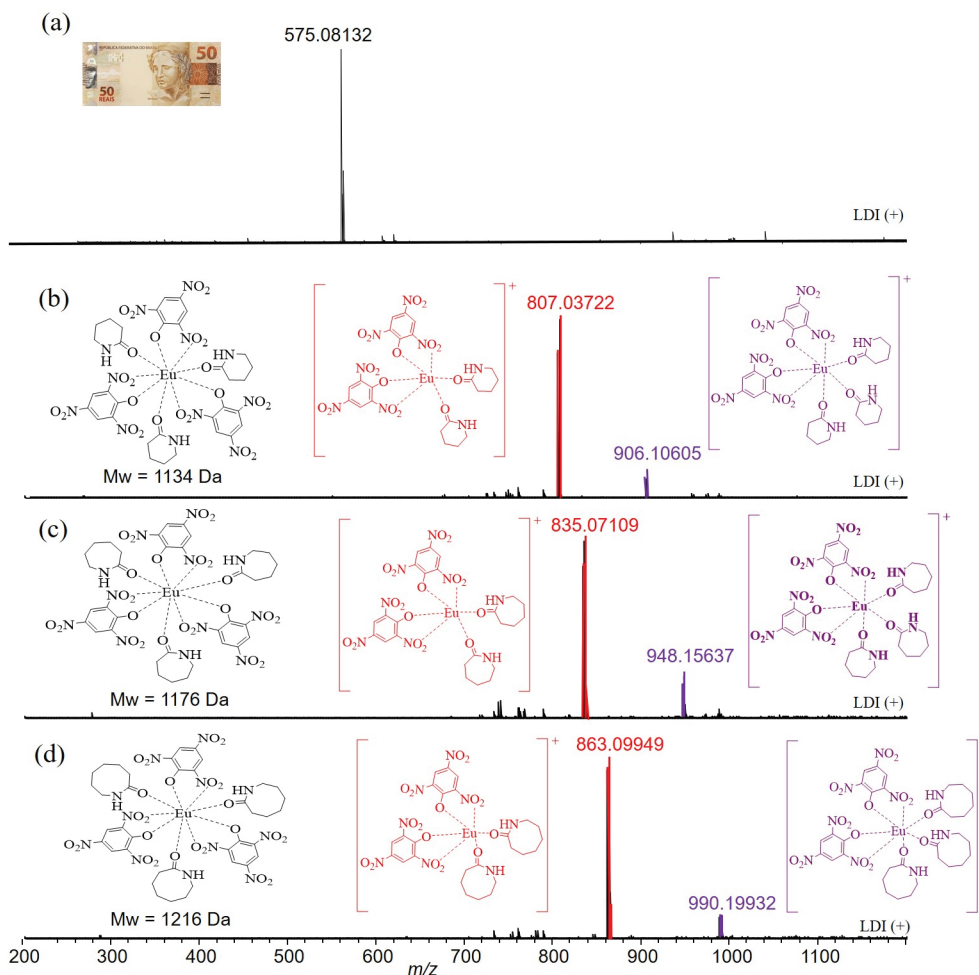

Figure 6. Chemical profile of R\$50 banknotes obtained by LDI (+) MS (a) without Eu^{III} complexes, and with (b) [Eu(pic)$_3$·(DVL)$_3$], (c) [Eu(pic)$_3$·(EPK)$_3$], and (d) [Eu(pic)$_3$·(OEN)$_3$].

Table 2. Molecular formulas, measured and theoretical mass values, mass errors, and DBE for $[Eu(pic)_3 \cdot (DVL)_3]$, $[Eu(pic)_3 \cdot (EPK)_3]$, and $[Eu(pic)_3 \cdot (OEN)_3]$ complexes identified by LDI (+) MS

Compound	Molecular formula	*m/z* measured	*m/z* theoretical	Error / ppm	DBE
$[Eu(pic)_3 \cdot (DVL)_3]$	$[EuC_{27}H_{31}N_9O_{17}]^+$	906.10605	906.10502	1.13	17
	$[EuC_{22}H_{22}N_8O_{16}]^+$	807.03722	807.03660	0.76	16
$[Eu(pic)_3 \cdot (EPK)_3]$	$[EuC_{30}H_{37}N_9O_{17}]^+$	948.15637	948.15197	4.64	17
	$[EuC_{24}H_{26}N_8O_{16}]^+$	835.07109	835.06790	3.82	16
$[Eu(pic)_3 \cdot (OEN)_3]$	$[EuC_{33}H_{43}N_9O_{17}]^+$	990.19932	990.19892	0.40	17
	$[EuC_{26}H_{30}N_8O_{16}]^+$	863.09949	863.09920	0.33	16

DBE: double bond equivalent; pic: picrate anion; DVL: delta-valerolactam; EPK: epsilon-caprolactam; OEN: oenantholactam.

(DBE) = 17, which represents the loss of a picrate molecule in the form of picric acid, $C_6H_3N_3O_7$ (228 Da) from the original formula, thus allowing the ionization to occur. An ion of *m/z* 807.03722, $[EuC_{22}H_{22}N_8O_{16}]^+$, DBE = 16 is also observed, which originates from the loss of a DVL molecule, M = C_5H_9NO (99 Da), from the ion of *m/z* 906.10605.

For the $[Eu(pic)_3 \cdot (EPK)_3]$ complex (Figure 6c), for which M = $EuC_{36}H_{39}N_{12}O_{24}$ and M_w = 1176 Da, the loss of a picrate molecule in the form of picric acid, M = $C_6H_3N_3O_7$ (228 Da), is detected, forming an ion of *m/z* 948.15637, $[EuC_{30}H_{37}N_9O_{17}]^+$, and DBE = 17. The formation of an ion of *m/z* 835.07109, $[EuC_{24}H_{26}N_8O_{16}]^+$, and DBE = 16 was also observed, originating from the loss of an EPK molecule, M = $C_5H_{11}NO$ (M_w = 113 Da), from the ion of *m/z* 948.15637.

For the $[Eu(pic)_3 \cdot (OEN)_3]$ complex, with M = $EuC_{39}H_{45}N_{12}O_{24}$ and M_w = 1216 Da, LDI (+) MS analysis (Figure 6d) shows that the loss of a picrate molecule in the form of picric acid, M = $C_6H_3N_3O_7$ (M_w = 228 Da), produces an ion of *m/z* 990.19932, $[EuC_{33}H_{43}N_9O_{17}]^+$, and DBE = 17. The signal observed at *m/z* 863.09949, $[EuC_{26}H_{30}N_8O_{16}]^+$, and DBE = 16 originated from the loss of an OEN molecule, M = $C_7H_{13}NO$ (127 Da).

LDI mass spectra in negative ionization mode, i.e., LDI (−) MS, for three complexes are shown in Figure S3 (SI section), presenting the same chemical profiles, which identify only the presence of the signal related to the ion of *m/z* 1064.87567, $[EuC_{24}H_8N_{12}O_{28}]^-$ with error = 2.48 ppm and DBE = 27. The results obtained by LDI (−) MS for the three complexes, shown in Figure S3, resembled the ESI (−) Fourier transform ion cyclotron resonance (FT-ICR) MS chemical profile of a europium picrate complex with *N*-methylcaprolactam, M = $Eu(PIC)_3(NMK)_3$, and an ion of *m/z* 1064.87567, $[EuC_{24}H_8N_{12}O_{28}]^-$, as reported by Destefani *et al.*[83] For the LDI (±) mass spectra of the banknotes marked with complexes, the signal of the ion of *m/z* 575.08132 (unmarked banknote) has been suppressed by signals coming from the complexes.

The isotopologue patterns of the experimental and theoretical signals of *m/z* 906.10605, 807.03722, 948.15637, 835.07109, 990.19932, and 863.09949 in the LDI (+) MS spectra (Figure 7) were compared and showed good agreement, thus confirming the presence of Eu^{III} complexes in the studied banknotes.

Conclusions

In this study, the $[Eu(pic)_3 \cdot (DVL)_3]$, $[Eu(pic)_3 \cdot (EPK)_3]$, and $[Eu(pic)_3 \cdot (OEN)_3]$ complexes were shown as new potential luminescent security materials for application in questioned documents. The identification of the complexes on the banknotes can be easily performed because wavelengths in the UV region can be used to produce light emission by the complexes. It was also possible to identify the complexes present on the surface of the banknotes using the non-destructive LDI (±) MS technique. Finally, the average cost for the synthesis of the complexes was R$0.65 *per* mg.

Supplementary Information

Supplementary data (UV-Vis, excitation spectra, and LDI (−) MS) are available free of charge at http://jbcs.sbq.org.br as a PDF file.

Acknowledgments
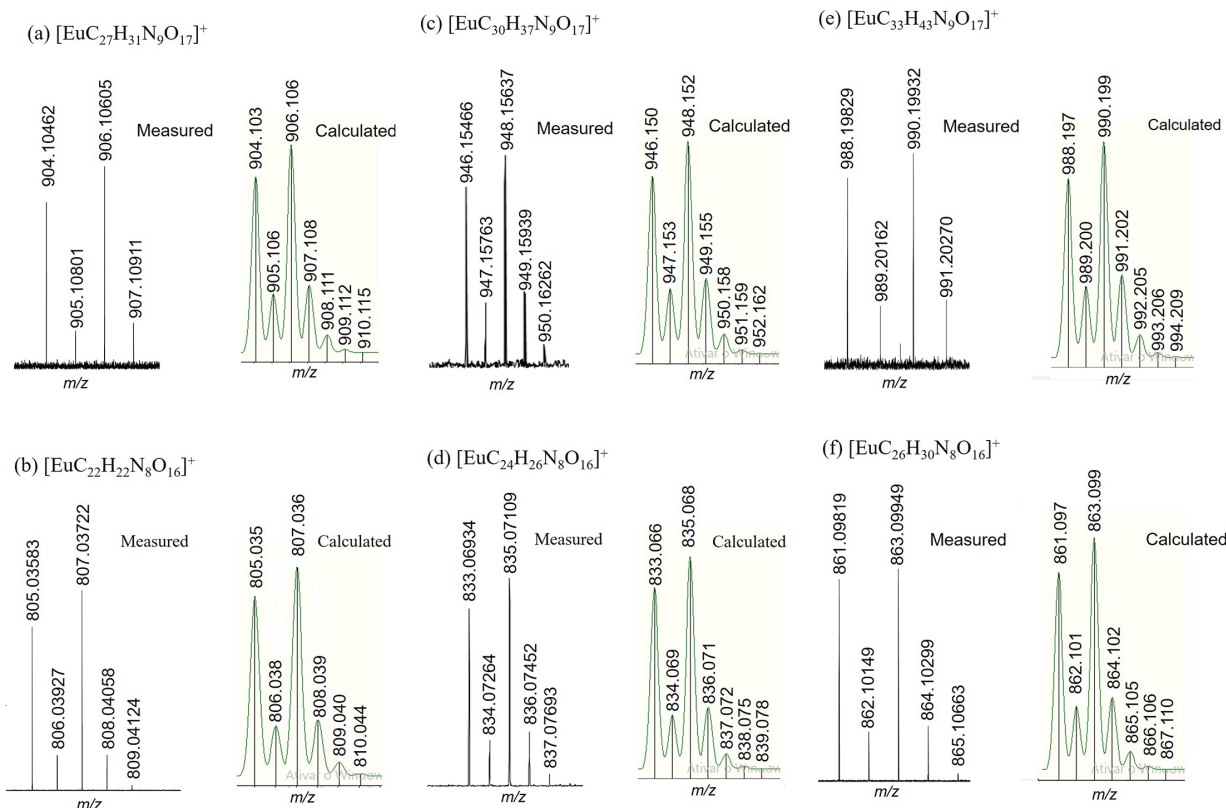
Figure 7. Experimental and calculated isotopologue patterns of (a) $[EuC_{27}H_{31}N_9O_{17}]^+$, (b) $[EuC_{22}H_{22}N_8O_{16}]^+$, (c) $[EuC_{30}H_{37}N_9O_{17}]^+$, (d) $[EuC_{24}H_{26}N_8O_{16}]^+$, (e) $[EuC_{33}H_{43}N_9O_{17}]^+$, and (f) $[EuC_{26}H_{30}N_8O_{16}]^+$ complexes.

Author Contributions

Clebson de J. Macrino was responsible for the conceptualization, data curation, formal analysis, investigation, methodology, visualization, writing the original draft, review, and editing; Elias M. Silva for the conceptualization, data curation, formal analysis, investigation, methodology, visualization, writing the original draft, and review; Victor R. Cunha for the formal analysis, investigation, and writing the original draft; Victor R. Fonseca for the formal analysis, investigation, and writing the original draft; Álvaro Cunha Neto for the conceptualization, data curation, formal analysis, investigation, methodology, visualization, writing the original draft, and review; Joyce R. Araújo for the formal analysis, investigation, and writing the original draft; Valdemar Lacerda Jr. and Wanderson Romão were responsible for the conceptualization, funding acquisition, investigation, methodology, project administration, resources, supervision, visualization, writing the original draft, review, and editing.

References

1. Valderrama, L.; Valderrama, P.; *Chemom. Intell. Lab. Syst.* **2016**, *156*, 188.

2. Hoyo-Meléndez, J. M.; Gondko, K.; Mendys, A.; Król, M.; Klisinska-Kopacz, A.; Sobczyk, J.; Jaworucka-Drath, A.; *Forensic Sci. Int.* **2016**, *266*, 329.

3. Bozicevic, M. S.; Gajovic, A.; Zjakic, I.; *Forensic Sci. Int.* **2012**, *223*, 314.

4. Saini, K.; Kaur, S.; *Egypt. J. Forensic Sci.* **2016**, *6*, 317.

5. Herrero, L. O.; Blanco, M. E.; García-Ruiz, C.; Bartolomé, L.; *J. Anal. Appl. Pyrolysis* **2018**, *131*, 9.

6. Silva, C. S.; Pimentel, M. F.; Amigo, J. M.; Ruiz, C. G.; Ojeda, F. O.; *Anal. Chim. Acta* **2018**, *1031*, 28.

7. Kaur, R.; Saini, K.; Sood, N. C.; *Sci. Justice* **2013**, *53*, 212.

8. Silva, V. A. G.; Talhavini, M.; Peixoto, I. C. F.; Zacca, J. J.; Maldaner, A. O.; Braga, J. W. B.; *Microchem. J.* **2014**, *116*, 235.

9. Joshi, M. C.; Kumar, A.; Thakur, S.; *Probl. Forensic Sci.* **2011**, *56*, 162.

10. Brandão, J. M. O. B.; Almeida, N. S. M.; Dixini, P. V. M.; Baier, C. H. A.; Dias, H. P.; Bassane, J. F. P.; França, H. S.; Silva, S. R. C.; Aquije, G. M. F. V.; Romão, W.; *Anal. Methods* **2016**, *8*, 771.

11. Correia, R. M.; Domingos, E.; Tosato, F.; Aquino, L. F. M.; Fontes, A. M.; Cao, V. M.; Filgueiras, P. R.; Romão, W.; *Forensic Chem.* **2018**, *8*, 57.

12. Braz, A.; López, M. L.; Ruiz, C. G.; *Forensic Sci. Int.* **2013**, *232*, 206.

13. Teixeira, C. A.; Poppi, R. J.; *Microchem. J.* **2019**, *144*, 411.

14. Almeida, M. R.; Correa, D. N.; Rocha, W. F. C.; Scafi, F. J. O.; Poppi, R. J.; *Microchem. J.* **2013**, *109*, 170.

15. Marise, C.; Ross, P.; *Forensic Sci. Int.* **2011**, *206*, 207.

16. Williams, M. R.; Moody, C.; Arceneaux, L. A.; Rinke, C.; White, K.; Sigman, M. E.; *Forensic Sci. Int.* **2009**, *191*, 97.

17. Correa, D. N.; Zacca, J. J.; Rocha, W. F. C.; Borges, R.; Souza, W.; Augusti, R.; Eberlin, M. N.; Vendramini, P. H.; *Forensic Sci. Int.* **2016**, *260*, 22.

18. Gallidabino, M.; Weyermann, C.; Marquis, R.; *Forensic Sci. Int.* **2011**, *204*, 169.

19. Weyermann, C.; Kirsch, D.; Vera, C. C.; Spengler, B.; *J. Am. Soc. Mass Spectrom.* **2006**, *17*, 297.

20. Domingos, E.; Carvalho, T. C.; Pereira, I.; Vasconcelos, G. A.; Thompson, C. J.; Augusti, R.; Rodrigues, R. R. T.; Tose, L. V.; Santos, H.; Araujo, J. R.; Vaz, B. G.; Romão, W.; *Anal. Methods* **2017**, *9*, 4400.

21. Ferreira, P. S.; Silva, D. F. A.; Augusti, R.; Piccin, E.; *Analyst* **2015**, *140*, 811.

22. Eberlin, L. S.; Haddad, R.; Neto, R. C. S.; Cosso, R. G.; Maia, D. R. J.; Maldaner, A. O.; Zacca, J. J.; Sanvido, G. B.; Romão, W.; Vaz, B. G.; Ifa, D. R.; Dill, A.; Cooks, R. G.; Eberlin, M. N.; *Analyst* **2010**, *135*, 2533.

23. Ifa, D. R.; Wiseman, J. M.; Song, Q.; Cooks, R. G.; *Int. J. Mass Spectrom.* **2007**, *259*, 8.

24. Schmidt, E. M.; Franco, M. F.; Regino, K. G.; Lehmann, E. L.; Arruda, M. A. Z.; Rocha, W. F. C.; Borges, R.; Souza, W.; Eberlin, M. N.; Correa, D. N.; *Sci. Justice* **2014**, *54*, 459.

25. Jara, M. A. Z.; Obregón, C. L.; del Castillo, C. A.; *Appl. Radiat. Isot.* **2018**, *135*, 212.

26. Guo, H.; Yin, B.; Zhang, J.; Quan, Y.; Shi, G.; *Forensic Sci. Int.* **2016**, *266*, 43.

27. Oliveira, V. S.; Honorato, R. S.; Honorato, F. A.; Pereira, C. F.; *Forensic Sci. Int.* **2018**, *286*, 121.

28. He, N.; Gao, M.; Shen, D.; Li, H.; Han, Z.; Zhao, P.; *Forensic Sci. Int.* **2019**, *297*, 1.

29. Shao, J.; Yan, J.; Li, X.; Li, S.; Hu, T.; *Dyes Pigm.* **2019**, *160*, 555.

30. Serwy, I. B.; Wanderley, K. A.; Lucena, M. A. M.; Maldaner, A. O.; Talhavini, M.; Rodrigues, M. O.; Weber, I. T.; *J. Lumin.* **2018**, *200*, 24.

31. Lucena, M. A. A.; Arouca, A. M.; Talhavini, M.; Alves-Júnior, S.; Weber, I. T.; *Microchem. J.* **2019**, *145*, 539.

32. Silva, J. Y. R.; Luz, L. L.; Maurício, F. G. M.; Alves, I. B. V.; Ferro, J. N. S.; Barreto, E.; Weber, I. T.; Azevedo, W. M.; Junior, S. A.; *ACS Appl. Mater. Interfaces* **2017**, *9*, 16458.

33. Maurício, F. G. M.; Pralon, A. Z.; Talhavini, M.; Rodrigues, M. O.; Weber, I. T.; *Forensic Sci. Int.* **2017**, *275*, 8.

34. Arouca, A. M.; Lucena, M. A. M.; Rossiter, R. J.; Talhavini, M.; Weber, I. T.; *Forensic Sci. Int.* **2017**, *281*, 161.

35. Lucena, M. A. M.; Ordoñez, C.; Weber, I. T.; Torre, M.; Ruiz, C. G.; López, M. L.; *Forensic Sci. Int.* **2017**, *280*, 95.

36. Lucena, M. A. M.; Rodrigues, M. O.; Gatto, C. C.; Talhavini, M.; Maldaner, A. O.; Alves Jr., S.; Weber, I. T.; *J. Lumin.* **2016**, *170*, 697.

37. Lucena, M. A. M.; Oliveira, M. F. L.; Arouca, A. M.; Talhavini, M.; Ferreira, E. A.; Alves, S.; Souza, F. H. V.; Weber, I. T.; *ACS Appl. Mater. Interfaces* **2017**, *9*, 4691.

38. Weissman, S. J.; *J. Chem. Phys.* **1942**, *10*, 214.

39. Andrade, A. V. M.; da Costa Jr., N. B.; Simas, A. M.; Longo, R. L.; Malta, O. L.; Sá, G. F.; *Quim. Nova* **1998**, *21*, 51.

40. Martins, T. S.; Isolani, P. C.; *Quim. Nova* **2005**, *28*, 111.

41. Liu, N.; *Inorg. Chem. Commun.* **2019**, *103*, 113.

42. Hong, Z.; Li, W.; Zhao, D.; Liang, C.; Liu, X.; Peng, J.; Zhao, D.; *Synth. Met.* **1999**, *104*, 165.

43. Wang, S.; Wang, L.; *TrAC, Trends Anal. Chem.* **2014**, *62*, 123.

44. Tu, D.; Zheng, W.; Liu, Y.; Zhu, H.; Chen, X.; *Coord. Chem. Rev.* **2014**, *273*, 13.

45. Guo, L.; Zhang, X.; Yang, D.; Liang, H.; Wang, Y.; *J. Lumin.* **2019**, 116610.

46. Xiang, W.; Wang, Z.; Kubicki, D. J.; Tress, W.; Luo, J.; Prochowicz, D.; Akin, S.; Emsley, L.; Zhou, J.; Dietler, G.; Gratzel, M.; Hagfeldt, A.; *Joule* **2019**, *3*, 205.

47. Koshelev, D. S.; Chikineva, T. Y.; Kozhevnikova, V. Y.; Medvedko, A. V.; Vashchenko, A. A.; Goloveshkin, A. S.; Tsymbarenko, D. M.; Averin, A. A.; Meschkov, A.; Schepers, U.; Vatsadze, S. Z.; Utochnikova, V. V.; *Dyes Pigm.* **2019**, *170*, 107604.

48. Park, S. J.; Je, B. S.; Jang, J. W.; Oh, M. S.; Koo, M. S.; Yang, S. J.; Yang, H. K.; *J. Alloys Compd.* **2019**, *789*, 367.

49. Shahi, P. K.; Singh, P.; Singh, A. K.; Singh, S. K.; Rai, S. B.; Prakash, R.; *J. Colloid Interface Sci.* **2017**, *491*, 199.

50. Silva, M. A.; Campos, N. R.; Ferreira, L. A.; Flores, L. S.; Júnior, J. C. A.; Santos, G. L.; Correa, C. C.; Santos, T. C.; Ronconi, C. M.; Colaço, M. V.; Simões, T. R. G.; Marques, L. F.; Marinho, M. V.; *Inorg. Chim. Acta* **2019**, *495*, 118967.

51. Junior, J. C. A.; Santos, G. L.; Colaco, M. C.; Barroso, R. C.; Ferreira, F. F.; Santos, M. V.; Campos, N. R.; Jesus, L. T.; Freire, R. O.; Marques, L. F.; *J. Phys. Chem. C* **2020**, *124*, 9996.

52. Silva, A. G.; Vicentini, G.; Zukerman-Schpector, J.; Castellano, E. E.; *J. Alloys Compd.* **1995**, *225*, 354.

53. Miranda Jr., P.; Carvalho, C. C.; Zukerman-Schpector, J.; Isolani, P. C.; Vicentini, G.; Zinner, L. B.; *J. Alloys Compd.* **2000**, *303*, 162.

54. Melo, C. V. P.; Vicentini, G.; Isolani, P. C.; Zukerman-Schpector, J.; Castellano, E. E.; *J. Alloys Compd.* **1998**, *275*, 242.

55. Nunes, C. C. F.; Zinner, K.; Zinner, L. B.; Carvalho, C. C.; Zukerman-Schpector, J.; Vicentini, G.; *Inorg. Chim. Acta* **1999**, *292*, 249.

56. Marinho, E. P.; Melo, D. M. A.; Zinner, L. B.; Vicentini, G.; Zukerman-Schpector, J.; Zinner, K.; *J. Alloys Compd.* **2000**, *303*, 116.

57. Destefani, C. A.; Motta, L. C.; Costa, R. A.; Macrino, C. J.; Bassane, J. F. P.; Filho, J. F. A.; Silva, E. M.; Greco, S.

J.; Carneiro, M. T. W. D.; Endringer, D. C.; Romão, W.; *Microchem. J.* **2016**, *124*, 195.

58. Lyle, S. J.; Rahaman, M. M.; *Talanta* **1963**, *10*, 1177.

59. Nakagawa, K.; Amita, K.; Mizuno, H.; Inoue, Y.; Hakushi, T.; *Bull. Chem. Soc. Jpn.* **1987**, *60*, 2037.

60. Marinho, E. P.; Melo, D. M. A.; Zinner, L. B.; Zinner, K.; Matos, J. E. X.; *J. Alloys Compd.* **1998**, *275*, 795.

61. Assunção, L. M.; Ionashiro, M.; Rasera, D. E.; Giolito, I.; *Thermochim. Acta* **1993**, *219*, 225.

62. Saleh, M. I.; Kusrini, E.; Fun, H. K.; Yamin, B. M.; *J. Organomet. Chem.* **2008**, *693*, 2561.

63. Martins, T. S.; Araujo, A. A. S.; Araujo, M. P. B. M.; Isolani, P. C.; Vicentini, G.; *J. Alloys Compd.* **2002**, *344*, 75.

64. Wang, Y. W.; Liu, W. S.; Tang, N.; Tan, M. Y.; Yu, K. B.; *J. Mol. Struct.* **2003**, *660*, 41.

65. Marinho, E. P.; Melo, D. M. A.; Zinner, L. B.; Zinner, K.; Castellano, E. E.; Schpector, J. Z.; Isolani, P. C.; Vicentin, G.; *Polyhedron* **1997**, *16*, 3519.

66. Carnall, W. T.; Fields, P. R.; Rajnak, K.; *J. Chem. Physics* **1968**, *49*, 4450.

67. Forsberg, J. H.; *Coord. Chem. Rev.* **1973**, *10*, 195.

68. Ferreira, R. A. S.; Nobre, S. S.; Granadeiro, C. M.; Nogueira, H. I. S.; Carlos, L. D.; Malta, O. L.; *J. Lumin.* **2006**, *121*, 561.

69. Sá, G. F.; Malta, O. L.; Donegá, C. M.; Simas, A. M.; Longo, R. L.; Santa-Cruz, P. A.; Silva Jr., E. F.; *Coord. Chem. Rev.* **2000**, *196*, 165.

70. Borges, A. S.; Fulgêncio, F.; Silva, J. G.; Santos, T. A. R.; Diniz, R.; Windmöller, D.; Magalhães, W. F.; Araujo, M. H.; *J. Lumin.* **2019**, *205*, 72.

71. Pavithran, R.; Kumar, N. S. S.; Biju, S.; Reddy, M. L. P.; Junior, S. A.; Freire, R. O.; *Inorg. Chem.* **2006**, *45*, 2184.

72. Costa, J. A. S.; Jesus, R. A.; Dorst, D. D.; Pinatti, I. M.; Oliveira, L. M. R.; Mesquita, M. E.; Paranhos, C. M.; *J. Lumin.* **2017**, *192*, 1149.

73. Borges, A. S.; Caliman, E. V.; Dutra, J. D. L.; Silva, J. G.; Araujo, M. H.; *J. Lumin.* **2016**, *170*, 654.

74. Borges, A. S.; Silva, J. G.; Ayala, J. D.; Dutra, J. D. L.; Speziali, N. L.; Brito, H. F.; Araujo, M. H.; *Spectrochim. Acta, Part A* **2014**, *117*, 718.

75. Santa-Cruz, P. A.; Teles, F. S.; *Spectra Lux Software v.1.0*; Ponto Quântico Nanodispositivos/ RENAMI, Recife, PE, Brazil, 2003.

76. Venturini Filho, E.; de Sousa Filho, P. C.; Serra, O. A.; Weber, I. T.; Lucena, M. A. M.; Luz, P. P.; *J. Lumin.* **2018**, *202*, 89.

77. Almeida, C. M.; Sales, D. D.; Tosato, F.; Santos, N. A.; Filho, J. F. A.; Macrino, C. J.; Pinto, F. E.; Filgueiras, P. R.; Romão, W.; *Microchem. J.* **2019**, *148*, 220.

78. Santos, N. A.; Souza, L. M.; Pinto, F. E.; Macrino, C. J.; Almeida, C. M.; Merlo, B. B.; Filgueiras, P. R.; Ortiz, R. S.; Borges, R. M.; Romão, W.; *Anal. Methods* **2019**, *11*, 1764.

79. Almeida, C. M.; Pinto, F. E.; Santos, N. A.; Souza, L. M.; Merlo, B. B.; Thompson, C. J.; Romão, W.; *Microchem. J.* **2019**, *149*, 104002.

80. Falco, L. F. G.; Melo, C. F. O. R.; Oliveira, D. N.; Guerreiro, T. M.; Catharino, R. R.; *Talanta* **2019**, *197*, 92.

81. Schmidt, E. M.; Franco, M. F.; Cuelbas, C. J.; Zacca, J. J.; Rocha, W. F. C.; Borges, R.; Souza, W.; Sawaya, A. C. H. F.; Eberlin, M. N.; Correa, D. N.; *Sci. Justice* **2015**, *55*, 285.

82. Colati, K. A. P.; Dalmaschio, G. P.; Castro, E. V. R.; Gomes, A. O.; Vaz, B. G.; Romão, W.; *Fuel* **2013**, *108*, 647.

83. Destefani, C. A.; Motta, L. C.; Vanini, G.; Souza, L. M.; Filho, J. F. A.; Macrino, C. J.; Silva, E. M.; Greco, S. J.; Endringer, D. C.; Romão, W.; *Microchem. J.* **2014**, *116*, 216.